

# Large-Scale Suspended Graphene Used as a Transparent Substrate for Infrared Spectroscopy

Hai Hu, Baoxing Liao, Xiangdong Guo, Debo Hu, Xiaofen Qiao, Ning Liu, Ruina Liu, Ke Chen, Bing Bai, Xiaoxia Yang,\* and Qing Dai\*

*Due to weak interactions between micrometer-wavelength infrared (IR) light and nanosized samples, a high signal to noise ratio is a prerequisite in order to precisely characterize nanosized samples using IR spectroscopy. Traditional micrometer-thick window substrates, however, have considerable IR absorption which may introduce unavoidable deformations and interruptions to IR spectra of nanoscale samples. A promising alternative is the use of a suspended graphene substrate which has ultrahigh IR transmittance (>97.5%) as well as unique mechanical properties. Here, an effective method is presented for fabrication of suspended graphene over circular holes up to 150  $\mu\text{m}$  in diameter to be utilized as a transparent substrate for IR spectroscopy. It is demonstrated that the suspended graphene has little impact on the measured IR spectra, an advantage which has led to the discovery of several missing vibrational modes of a 20 nm thick PEO film measured on a traditional  $\text{CaF}_2$  substrate. This can provide a better understanding of molecules' fine structures and status of hanging bands. The unique optical properties of suspended graphene are determined to be superior to those of conventional IR window materials, giving this new substrate great potential as part of a new generation of IR transparent substrates, especially for use in examining nanoscale samples.*

Infrared spectroscopy (IR) directly probes the vibrational modes of molecules in the mid-IR spectral region,  $\approx 2.5\text{--}25\ \mu\text{m}$  ( $4000\text{--}400\ \text{cm}^{-1}$ ),<sup>[1]</sup> and has been widely used for chemical detection,<sup>[2]</sup> food safety,<sup>[3]</sup> and biosensing.<sup>[4]</sup> However, this method is limited for use in examining nanoscale materials because the wavelengths of mid-IR light are almost three orders of magnitude larger than the size of nanoscale molecules ( $\approx 10\ \text{nm}$ ). This leads to remarkably small and difficult

to detect light–molecule interactions.<sup>[5–8]</sup> Furthermore, measurement results are seriously deteriorated by the absorption (>5%) due to traditional IR window materials such as  $\text{CaF}_2$ , KBr, and Ge, which are comparable to, or even larger than, signals of nanoscale matter. In particular, IR transmittance through these window materials declines sharply near their cutoff regions, causing even more severe interference.<sup>[9]</sup> One potential solution to decrease the absorption of these traditional IR window materials would be to decrease their thickness to smaller than several micrometers, however, this is difficult due to the fragile nature of the IR window materials as well as the necessary double-side mechanical polishing process.<sup>[10,11]</sup> In addition, traditional windows are highly susceptible to degradation due to water, which prohibits the use of these materials in all but the most benign environments.<sup>[12,13]</sup> For these reasons, a search is ongoing for novel IR window materials that have limited absorption across the whole mid-IR spectral region and can also be applied to more severe and wet environments.

Suspended graphene is a potentially ideal transparent substrate for IR spectroscopy mainly due to its very limited

H. Hu, B. X. Liao, X. D. Guo, Dr. D. B. Hu,  
Dr. X. F. Qiao, N. Liu, R. N. Liu, K. Chen,  
B. Bai, Prof. X. X. Yang, Prof. Q. Dai  
Division of Nanophotonics  
CAS Center for Excellence in Nanoscience  
National Center for Nanoscience and Technology  
Beijing 100190, P. R. China  
E-mail: yangxx@nanoctr.cn; daiq@nanoctr.cn  
H. Hu, Prof. Q. Dai  
University of Chinese Academy of Sciences  
Beijing 100049, P. R. China  
DOI: 10.1002/sml.201603812



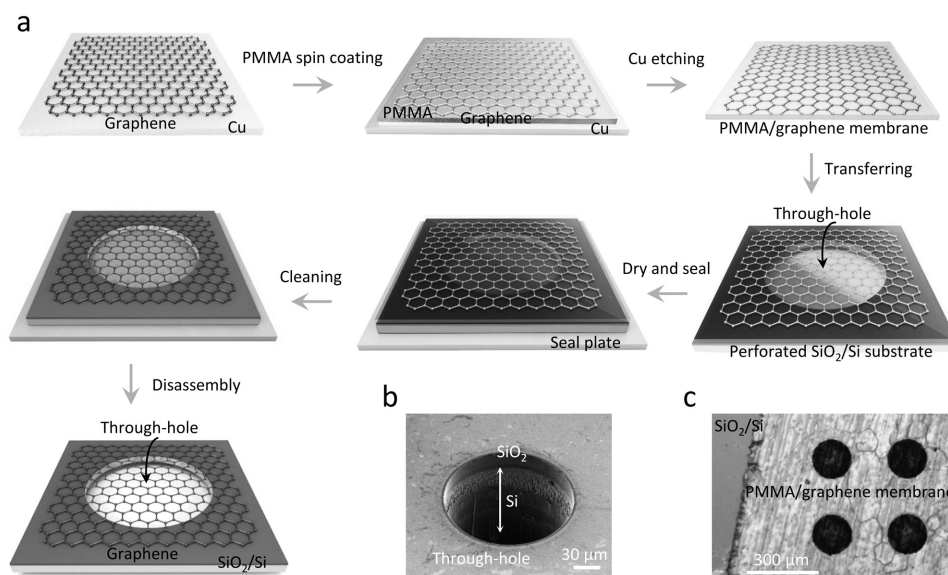


**Figure 1.** Transferring procedure used during fabrication of ultralarge area suspended graphene membranes. a) Suspended CVD graphene was fabricated using typical procedures, including polymethyl methacrylate (PMMA) spin-coating, copper foil etching, rinsing, and wet-transfer onto a perforated  $\text{SiO}_2$  substrate. After the PMMA/graphene membrane was thoroughly dried, the back of the perforated substrate was blocked using a polytetrafluoroethylene (PTFE) seal plate in order to prevent liquid from becoming trapped in the capillary-like perforations on the substrate hole during drying once the PMMA support had been etched away. b) SEM image of the fabricated perforated  $\text{SiO}_2/\text{Si}$  substrate. c) Optical image of the PMMA/graphene membrane transferred onto a perforated  $\text{SiO}_2/\text{Si}$  substrate.

light absorption across the entire mid-IR and terahertz regions.<sup>[14–17]</sup> In the case of doped graphene in this regime, Pauli-blocking occurs and the optical absorption can be smaller than even the intrinsic absorption of graphene (2.3%).<sup>[18]</sup> Furthermore, suspended graphene is also chemically inert,<sup>[19]</sup> mechanically sturdy,<sup>[20]</sup> and waterproof, all properties needed for high-quality substrates. These extinction properties of suspended graphene have been widely demonstrated by previous applications, including ultimate permeation across a membrane,<sup>[21]</sup> use in microscale electro-mechanical systems oscillators, capacitive pressure sensors and biosensors, etc.<sup>[22–25]</sup> Unlike those applications which are based on suspended graphene only several micrometers in size, a prerequisite for use of graphene as a substrate for far-field IR spectroscopy is the fabrication of large area suspended graphene. This is because the mid-IR spectrum ranges from  $\approx 2.5$  to  $25 \mu\text{m}$  and the transmission efficiency of a single subwavelength aperture is predicted by Bethe to scale as  $(r/\lambda)$ , where  $r$  is the hole radius and  $\lambda$  is the wavelength of the incident light.<sup>[26,27]</sup>

Here, we present an effective method for fabrication of large-scale suspended graphene over circular holes up to  $150 \mu\text{m}$  in diameter. The IR spectra of a suspended monolayer, as well as several stacked layers of graphene, were characterized via Fourier transform infrared (FTIR) microscopy. The transmittance of both doped monolayer graphene and stacked few-layer graphene is over 97.5% across the entire mid-IR range, a better result than that of traditional IR window materials. This suspended graphene was used as supporting substrate for analytes in far-field FTIR measurements. Experimental results from the examination of a 20 nm thick polyethylene oxide (PEO) film analyte indicate that the suspended graphene has little impact on the measured

results. In contrast, under the same measurement conditions one of the best conventional IR windows,  $500 \mu\text{m}$  thick  $\text{CaF}_2$ , can interfere the measurement results due to a low signal to noise ratio. The unique optical properties of suspended graphene make it promising as part of a new generation of IR transparent substrate materials, particularly for measuring nanoscale samples.

The typical procedure for effective fabrication of suspended graphene membranes with large areas is shown in **Figure 1**. The graphene used in this work was synthesized using chemical vapor deposition (CVD) method. First, graphene that had been grown on copper foil was spin-coated with poly(methyl methacrylate) (PMMA) and the copper foil was then etched to free the PMMA/graphene layer.<sup>[28]</sup> Next, the graphene/PMMA layer was scooped up onto a perforated  $\text{SiO}_2$  substrate dotted with several through-holes a hundred microns in size. These fixed dimension holes had been fabricated using standard ultraviolet radiation photolithographic methods followed by dry etching, as shown in Figure 1b and Figure S1 (Supporting Information). After being thoroughly dried, the back of the perforated substrate was capped with a polytetrafluoroethylene (PTFE) seal plate that would prevent liquid from getting trapped in the capillary-like holes during the drying process after the PMMA support had been etched away. The PMMA layer was then washed off in heated acetone for half an hour before the sample was quickly placed into a low surface tension solvent, i.e., methoxynonafluorobutane ( $\text{C}_4\text{F}_9\text{OH}_3$ ). Multilayer graphene was made using layer-by-layer stacking before it was transferred onto perforated substrates (Figure S2, Supporting Information). Compared with previously used inverted floating methods, the use of heated acetone bath makes this transfer method more stable and more economical.<sup>[25,29]</sup> When using this method a

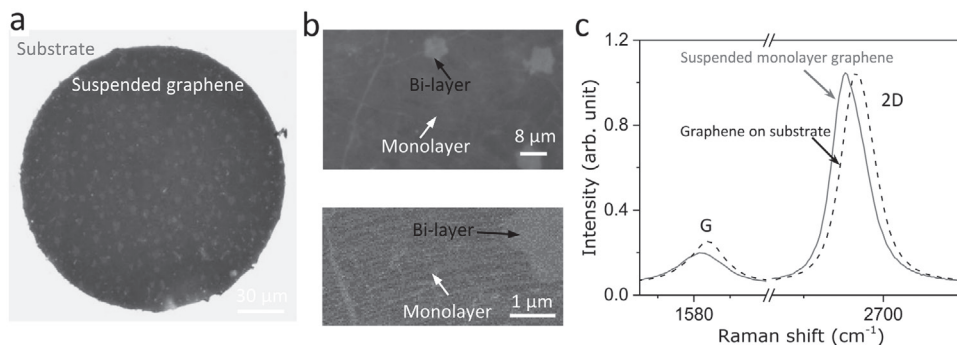


**Figure 2.** Characterization of large area suspended graphene membranes. a) Optical image of the suspended CVD monolayer graphene over a circular hole (150  $\mu\text{m}$  in diameter) in a  $\text{SiO}_2/\text{Si}$  substrate. b) A close-up optical image of the suspended CVD monolayer graphene (top) and a scanning electron microscope (SEM) image (bottom) of the suspended CVD graphene. The arrows indicate monolayer (white) and bilayer islands (black), respectively. c) Comparison of Raman spectra of the suspended CVD graphene and graphene on  $\text{SiO}_2$  substrate.

single transfer process can produce a batch of suspended graphene. This means that several holes can be covered by graphene during one procedure, such as the four holes indicated in Figure 1c and Figure S3 (Supporting Information).

The images in **Figure 2a,b** show monolayer graphene suspended over a circular hole 150  $\mu\text{m}$  in diameter. A close-up optical image (top of Figure 2b) and a scanning electron microscope image (bottom of Figure 2b) both show a variety of geometric features in the CVD graphene, including monolayer and bilayer islands. Raman spectra of these geometric features in suspended CVD graphene are shown in Figure 2c and Figure S4, and correspond to the areas indicated with arrows in the optical microscopy image (Figure 2b top). The Raman spectrum measured for the monolayer region of the suspended graphene membrane has a small D peak, indicating that this region was composed of high-quality CVD graphene. The peak width ( $\approx 15.3 \text{ cm}^{-1}$ ) of G mode of suspended graphene is broader than that ( $\approx 11.8 \text{ cm}^{-1}$ ) of supported graphene. The blueshift of the G and 2D peaks and broadening of G peak for supported graphene are attributed to the hole doping induced by the  $\text{SiO}_2$  substrate.<sup>[30]</sup> The ratio

of 2D and G peaks of suspended graphene is stronger than that of supported graphene, due to the extremely low charge impurity concentration in the former.<sup>[31]</sup> The Raman spectra and atomic force microscope (AFM) images measured in the region indicated with black arrow (Figure 2b) indicate that this area is bilayer graphene islands (Figure S4, Supporting Information).<sup>[32,33]</sup>

A far-field FTIR microscope with a detection area as small as  $5 \times 5 \mu\text{m}^2$  was used to characterize the analytes supported on the suspended graphene. The IR transmittance of both a monolayer and several stacked layers of suspended graphene was examined. As shown in **Figure 3a**, the IR spectra for the monolayer graphene had an ultrahigh transmittance ( $>97.5\%$ ) for the entire mid-IR spectral region. This low light absorption is due to the monolayer being only one atom thick as well as a lack of active IR vibrational modes because the graphene consists of like atoms. For comparison, the IR transmittance spectra of a 500  $\mu\text{m}$  thick  $\text{CaF}_2$  substrate (a typical IR window material) is also plotted in Figure 3a. Between 1000 and 6000  $\text{cm}^{-1}$  the transmittance of the  $\text{CaF}_2$  substrate is about 90%, however, there is a large decrease

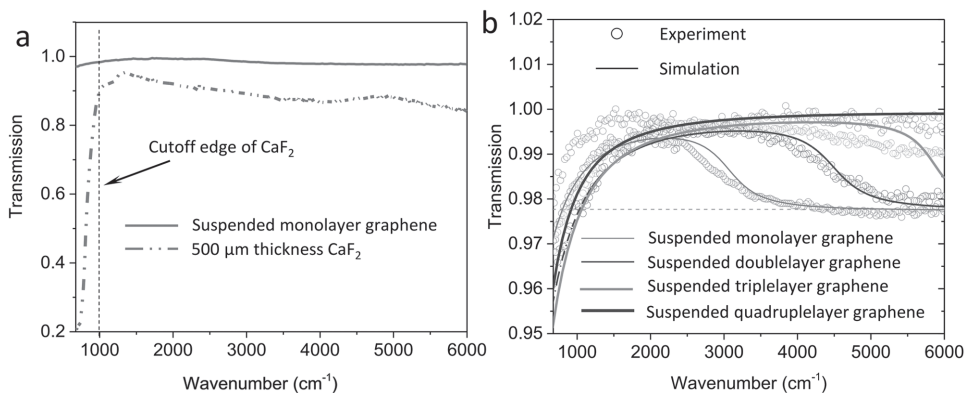


**Figure 3.** FTIR spectroscopy characterization of CVD graphene membranes suspended over large areas. a) Comparison of the transmission FTIR spectra of a suspended monolayer of graphene and a 500  $\mu\text{m}$  thick  $\text{CaF}_2$  substrate. The black dotted vertical line indicates the  $\text{CaF}_2$  cutoff edge. b) FTIR spectra of large area suspended graphene including a monolayer, double-layer, triple-layer, and quadruple-layer graphene. Circles indicate experiment results and lines indicate corresponding simulation results obtained using the finite element method. The light dashed horizontal line is to represent the intensity absorption at 2.3%. In the theoretical model, the thickness of the monolayer graphene film is 0.34 nm; the graphene surface conductivity was defined using the Kubo formula in a complex form consisting of both interband and intraband contributions; and the Fermi level was 0.2 eV in accordance with the Fermi level observed in the previous Raman result (Figure 2c). In the case of multilayer graphene calculations, each graphene layer was considered to have the same Fermi energy level, mobility and relaxation time.

**Table 1.** Comparison of a graphene substrate with several traditional IR window materials.

	Average transmittance @ [4000–1200 cm <sup>-1</sup> ]	Cutoff edge [cm <sup>-1</sup> ]	Water solubility [g per 100 g H <sub>2</sub> O] @ 25 °C
Graphene	97%	None	Insoluble
MgF <sub>2</sub>	90%	1500–400	0.0018
CaF <sub>2</sub>	92%	1100–400	0.0013
KBr	73%	None	53.5
ZnS	60%	800–400	0.00069
Ge	47%	600–400	Insoluble

below the cutoff edge at about 1000 cm<sup>-1</sup>, with transmittance at only 20% at 700 cm<sup>-1</sup>. A systematic comparison including three key parameters (average transmittance, cutoff edge, and water solubility) for suspended graphene and traditional IR window materials (MgF<sub>2</sub>, CaF<sub>2</sub>, KBr, ZnS, ZnSe, Si, and Ge) are listed in **Table 1**. The graphene substrate outperforms the traditional IR window materials across all properties, including transmittance (which could hardly be greater than 95% for traditional materials), cutoff edge, and how hygroscopic the material was.<sup>[12,13]</sup> Another advantage of the suspended monolayer graphene is that the tiny thickness of only one atomic layer has little or no effect on the IR light path. Furthermore, traditional IR window materials have millimeter-scale thicknesses and require cumbersome double-side mechanical polishing that may cause harmful reflection, refraction, and/or interference. Use of thin traditional window materials with thickness less than a few hundred micrometers is impeded by both their high fragility and the need for complex processing.

Isolated atomic planes can also be assembled using a precisely chosen sequence of layer-by-layer stacking. Figure 3b shows the FTIR spectra of graphene membranes one to four layers thick. The transmission spectrum of monolayer graphene exhibits a wide and gentle slope in the range below 1700 cm<sup>-1</sup>, as shown in Figure 3b. This feature appears due to the intraband transition of free carriers, an effect which is expected to increase as the Fermi energy ( $E_F$ ) moves away from the Dirac point. In the spectral range of interest, the conductivity of graphene follows the Drude model  $\sigma = \frac{ie^2(|E_F|)}{\hbar\pi(\omega + i/\tau)}$ .<sup>[34,35]</sup> For tightly stacked graphene layers (small layer separations), one can replace  $N$  parallel conductive layers by an equivalent layer having the sum of the  $N$  conductivities,  $\sigma = \sum_{a=1}^N \sigma^{(a)} = \frac{ie^2 \left( \sum_{a=1}^N |E_F^{(a)}| \right)}{\hbar\pi(\omega + i/\tau)}$ . This expression corresponds to the Drude conductivity for a graphene layer with Fermi level  $E_F^{NL} = \sum_{a=1}^N |E_F^{(a)}|$ .<sup>[36]</sup> Therefore, with an increase in the number of graphene layers the slope blue shifts because the Fermi energy is positively correlated with the number of graphene layers.<sup>[36–38]</sup> In spite of increases to the number of layers, there was little change to the amount of ultrahigh transmittance. Unlike mechanical exfoliated A–B stacked bilayer graphene which has a phonon absorption peak at 1580 cm<sup>-1</sup>, randomly stacked graphene has no IR active vibrational modes.<sup>[39,40]</sup> It is also worth noting that

the mechanical strength of the stacked multilayer graphene improved significantly. Graphene with perfect structure has been demonstrated to be the strongest material ever measured, showing ultrahigh Young's modulus ( $\approx 1$  TPa) and intrinsic strength ( $\approx 130$  GPa).<sup>[41]</sup> Typically, the mechanical properties could be measured via nanoindentation in AFM. Albeit featuring polycrystalline structure and thus containing grain boundaries that can potentially weaken the material, CVD graphene still exhibits a breaking strength of  $\approx 90$  GPa.<sup>[42,43]</sup> For artificially stacked few layers, the strength is further enhanced as their in-plane stiffness is proportional to the thickness.<sup>[44]</sup> This leads to two further advantages: high yield rates for graphene membranes suspended over large areas, and a large load capacity for analytes when the membranes are used as IR transparent substrate. In addition, compared with traditional IR window materials, suspended graphene is much more compatible with wet samples (Table 1).

Based on the results described above, the property of large area suspended CVD graphene membranes as transparent substrate for IR spectroscopy was investigated. **Figure 4a** shows a conceptual view of a suspended graphene membrane used as an IR transparent substrate. A nanoscale thick PEO film was used as analyte because of its ability to form a good film and its well-studied IR spectra.<sup>[45]</sup> Atomic force microscopy (AFM) analysis of the PEO-coated 4-layer graphene substrate revealed that the PEO film was about 20 nm thick, as shown in Figure 4b. Figure 4c shows a comparison of the IR absorption spectra for 20 nm thick PEO films coated onto a 4-layer graphene substrate versus a 500  $\mu\text{m}$  thick CaF<sub>2</sub> substrate. An FTIR microscope equipped with a mercury–cadmium–telluride detector was used to acquire 256 scans per data point with a spectral resolution of 4 cm<sup>-1</sup>. The suspended graphene with analyte coat was a circle 150  $\mu\text{m}$  in diameter, a size significantly larger than the IR beam (diameter,  $\approx 25$   $\mu\text{m}$ ) used in the experiments. The absorption spectra ( $1 - T/T_0$ ) were obtained using the transmittance of the bare substrate,  $T_0$ , as a reference.

As can be seen in Figure 4d, the absorption spectrum collected for 20 nm thick PEO on graphene was of high quality with a nearly horizontal baseline. This means that the suspended graphene substrate had virtually no impact on the measurement. In contrast, the absorption spectrum of a PEO film with the same thickness on a 500  $\mu\text{m}$  CaF<sub>2</sub> substrate was seriously affected by the heavily distorted background baseline of the CaF<sub>2</sub>, particularly in the fingerprint region ( $\approx 400$ – $1500$  cm<sup>-1</sup>) which happens to be the cutoff edge of CaF<sub>2</sub>. A close-up image of this spectral range in Figure 4e shows that the interference from the CaF<sub>2</sub> substrate could have severe consequences on the ability to observe some weak absorption peaks. In Figure 4d, there are several absorption peaks seen in the PEO spectrum taken on the graphene substrate that cannot be distinguished from noise using the CaF<sub>2</sub> substrate and are indicated with black Xs. Specifically, peaks at 844, 947, 966, 1342, 1358, and 1466 cm<sup>-1</sup> which represent  $r(\text{CH}_2)a$ ,  $r(\text{CH}_2)s-v(\text{COC})a$ ,  $r(\text{CH}_2)a$ ,  $\omega(\text{CH}_2)a$ ,  $\omega(\text{CH}_2)s+v(\text{CC})$ , and  $\delta(\text{CH}_2)a-\delta(\text{CH}_2)s$ , respectively.<sup>[45]</sup> The prefixes  $r$ ,  $v$ ,  $\omega$ , and  $\delta$  indicate rocking, stretching, wagging, and bending modes, respectively. The

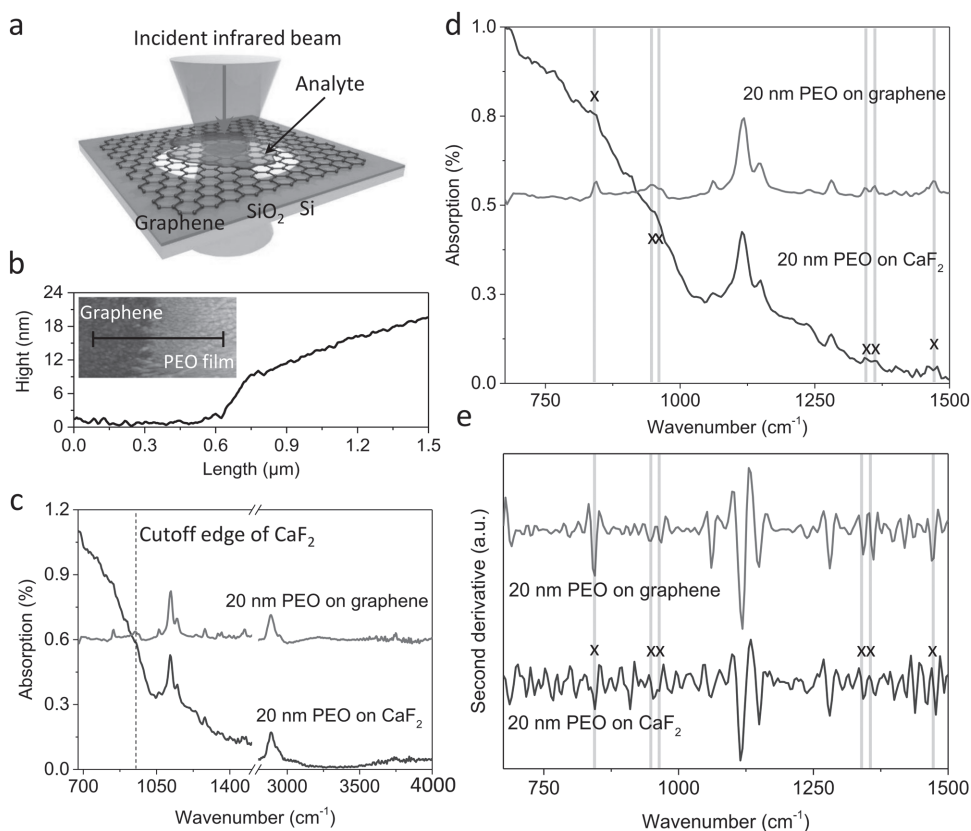


**Figure 4.** Investigation of suspended graphene used as a transparent substrate for IR spectroscopy. a) Conceptual view of suspended graphene used as a transparent substrate for IR spectroscopy. b) AFM analysis of a PEO film coated onto a 4-layer graphene substrate. The line-scan profile corresponds to the black line shown in the inset. c) IR absorption spectra of 20 nm PEO coated onto a 4-layer graphene substrate or a 500  $\mu\text{m}$   $\text{CaF}_2$  substrate. The black dotted vertical line indicates the cutoff edge of  $\text{CaF}_2$ . d) Close-up image of panel (c) from 675 to 1500  $\text{cm}^{-1}$ . e) The second derivative of the IR spectra shown in panel (d). The light vertical lines indicate various PEO molecular vibrational modes. Black Xs in panels (d) and (e) indicate PEO vibrational modes where the IR absorption signal is below the noise level and could not be distinguished using a 500  $\mu\text{m}$   $\text{CaF}_2$  substrate because of serious interference from the substrate.

suffixes s and a imply symmetric or antisymmetric modes with respect to the twofold axis perpendicular to the helix axis and passing through the oxygen atom or center of the C–C bond. The + and – signs denote the phase relationship for the potential energy distribution of the coupled coordinates. The second derivative of the IR spectra is shown in Figure 4e, and further confirms the results noted above. Every absorption peak in an IR spectrum represents a corresponding active IR vibrational mode and the collection of these modes constitutes the IR fingerprint of the analyzed molecules. Therefore, the absence of absorption peaks could cause problems for resolving spectra and producing reliable analyses and results. The unsatisfying results collected for PEO on the  $\text{CaF}_2$  substrate are mainly due to serious interference from the  $\text{CaF}_2$ . A typical IR measurement is not performed in situ, that is, the reference spectrum  $T_0$  is obtained from transmittance of the bare substrate as opposed to using the actual region of substrate underneath the sample. This is because the substrate is in direct contact with the analyte and therefore its specific IR spectrum would be difficult to measure. In general, the deviation between two different references  $T_0$  is much less than 0.002, a small value compared with the signals from micrometer and sub-micrometer samples, where absorbance generally exceeds 10%. However,

because of the strong absorption across the wide range of the cutoff region in  $\text{CaF}_2$  and some other traditional IR window materials, the deviation in our experiment approaches 0.002 (Figure S5, Supporting Information). The absorption deviation when using the 500  $\mu\text{m}$   $\text{CaF}_2$  window is on the same order of magnitude as the absorption peaks collected from nanoscale samples. This may cause interference with experimental results and impede better understanding of the fine structures of molecules. Overall, the single-atom-layer thick suspended graphene substrate has an ultrahigh transmittance, good chemical/thermostability, and great mechanical strength, and is therefore an ideal IR transparent substrate for IR spectral measurements of nanoscale samples.

Traditional hundred-micrometer-thick window substrates used for IR measurements have considerable IR absorptions and are incompatible with any moisture or liquid conditions, therefore, they do not satisfy the criteria necessary for use in nanoscale IR characterization. We have presented an effective method for fabricating large scale suspended graphene (150  $\mu\text{m}$  in diameter) which can be used as novel and thin transparent substrates for IR spectroscopy. This substrate demonstrated both ultrahigh IR transmittance (>97.5%) and unique mechanical properties. Experimental results demonstrated that the suspended graphene had little to no

impact on the measured IR spectra of a 20 nm thick PEO film sample. Furthermore, use of this substrate with the PEO sample gave a much higher quality IR spectrum than when a traditional  $\text{CaF}_2$  substrate was used, allowing for the discovery of several not previously detected vibrational modes. Because of its higher detection sensitivity and its excellent environmental compatibility, it could be widely used with integration of plasmon-enhanced IR absorption spectroscopy. Overall, the ability of the suspended graphene substrate to probe various molecular bonds of nanoscale samples gives it great potential for use in the characterization of various organic/inorganic nanofilms, biomolecules in moist conditions, electrochemical reactions on graphene surfaces, etc.

## Experiment Section

**Preparation of Perforated  $\text{SiO}_2/\text{Si}$  Substrate:** 250  $\mu\text{m}$  thick  $\text{SiO}_2/\text{Si}$  substrate with through-hole (150  $\mu\text{m}$  in diameter) was patterned by deep-UV lithography method (SUSS MA6 Mask Aligner) on  $\approx 6 \mu\text{m}$  thick 1150P positive photoresist (SUNTIFIC) for 15 min. Exposed 1150P was developed in SUN-238D (SUNTIFIC) developer solution for 2.5 min. The hole arrays were etched by  $\text{C}_4\text{F}_8$  and  $\text{SF}_6$  gases (NORTH MICROELECTRONICS, DSE200). Then, the photoresist layer was dissolved by acetone and the whole wafer is cleaned by isopropyl alcohol. The remaining residues on the silicon oxide surface were removed by oxygen plasma cleaning.

**Fabrication of Large Area Suspended Graphene:** Graphene was grown by chemical vapor deposition on copper and then transferred to the perforated  $\text{SiO}_2/\text{Si}$  substrate using an improved wet-transfer techniques. Before the transfer process, a PMMA layer was spin-coated on the upside of graphene/copper foil. Subsequently, the backside graphene was removed using oxygen plasma and the copper foil was selectively etched in 1:1 iron chloride ( $0.5 \text{ mol L}^{-1}$ ) and hydrochloric acid ( $0.5 \text{ mol L}^{-1}$ ) solution. The PMMA/graphene film floating on the etchant was cleaned by deionized water several times to rinse the etchant residue and then transferred onto the perforated  $\text{SiO}_2/\text{Si}$  substrate. Then, constant pressure nitrogen source blew the PMMA/graphene layer and heated the sample at 80  $^\circ\text{C}$  at the same time to make graphene perfectly attach onto  $\text{SiO}_2$  surface. After the PMMA/graphene membrane was thoroughly dried, the back of the perforated substrate was blocked using a PTEF seal plate in order to prevent liquid from becoming trapped in the capillary-like perforations on the substrate hole during drying once the PMMA support had been etched away. Finally, the PMMA layer was dissolved by acetone and the whole chip is cleaned by isopropyl alcohol and removed the sealed block on the back of the chip. For multiple layer graphene, the PMMA-coated graphene was directly transferred onto another layer graphene on copper foil with repeated layer-by-layer stacking.

**Preparation of PEO Film:** The PEO film was prepared by dispersing 1.5 g PEO ( $M_w = 100\,000$ ) in 60 mL acetonitrile. Then, the mixture was heated and maintained at 45  $^\circ\text{C}$  with stirring for 12 h to melt the PEO power completely. The solution was centrifuged at 1000 rpm for 20 min and the resulting clear supernatant was reserved. To form the PEO film, the clear solution was drop cast onto the graphene device followed by baking at 50  $^\circ\text{C}$  to remove residual acetonitrile.

**Characterization:** The Raman spectra of graphene were all acquired using a micro-Raman microscope (Horiba JobinYvon, LabRAM HR800) with an excitation laser wavelength of 514 nm and a spot size of  $\approx 1 \mu\text{m}$ . The thickness of PEO film was measured by AFM (Bruker, Dimension Icon) using tapping mode. The morphology of as prepared graphene and PEO film was characterized by scanning electron microscope (SEM, Hitachi, S-4800) operated at 1 kV. The IR transmission measurements of samples were performed with a Fourier transform infrared spectrometer with a microscopy (BRUKER, Vertex80v, Hyperion 2000). The transmission spectra of a bare through-hole was taken as background and then the transmission spectra of suspended graphene in the same area were acquired by automatically subtracting the background. The size range IR microscope studied was from about 10 to 200  $\mu\text{m}$  in this study. Each measurement was repeated several times to confirm the extinction spectrum. All measurements were performed at room temperature and atmospheric environment.

**Simulation Methods:** The absorption responses of suspended graphene are simulated by the finite element method. In the theoretical model, the thickness of the monolayer graphene film ( $t_g$ ) is 0.34 nm. The equivalent relative permittivity is derived from the 2D conductivity of graphene and is given by  $\varepsilon = i\sigma/\varepsilon_0\omega t_g$ .<sup>[46]</sup> Here,  $\varepsilon_0$  is the free space permittivity,  $\omega$  is the light angular frequency, and  $\sigma$  is the graphene conductivity calculated from the Kubo formula;<sup>[47]</sup> and the Fermi level was 0.2 eV in accordance with the Fermi level observed in the previous Raman result (Figure 2c). In the case of multilayer graphene calculations, each graphene layer was considered to have the same Fermi energy level, mobility, and relaxation time. The total conductivity still has the Drude form,  $\sigma^{1/4}_{\text{total}} = iD_{\text{total}}/\pi(\omega + iT)$ , where the sum of the Drude weights for  $N$  layer graphene  $D_{\text{total}} = N^{1/2}e^2E_F/\hbar$ , and the total Fermi level,  $E_F$ , was substituted by  $N^{1/2}E_F$ , where  $N$  is the number of graphene layers.<sup>[36–38]</sup>

## Supporting Information

Supporting Information is available from the Wiley Online Library or from the author.

## Acknowledgements

This work was supported by the National Basic Research Program of China (Grant Nos. 2015CB932400 and 2016YFA0201600), the National Natural Science Foundation of China (Grant Nos. 51372045, 11504063, and 11674073), the Bureau of International Cooperation, Chinese Academy of Sciences (Grant No. 121D11KYSB20130013), and the key program of the bureau of Frontier Sciences and Education Chinese Academy of Sciences (Grant No. QYZDB-SSW-SLH021).

## Conflict of Interest

The authors declare no conflict of interest.

- [1] B. Stuart, *Infrared Spectroscopy*, John Wiley & Sons, Inc., Hoboken, NJ, USA **2005**.
- [2] A. Bagri, C. Mattevi, M. Acik, Y. J. Chabal, M. Chhowalla, V. B. Shenoy, *Nat. Chem.* **2010**, *2*, 581.
- [3] L. J. Mauer, A. A. Chernyshova, A. Hiatt, A. Deering, R. Davis, *J. Agric. Food Chem.* **2009**, *57*, 3974.
- [4] F. Garczarek, K. Gerwert, *Nature* **2006**, *439*, 109.
- [5] F. Huth, A. Govyadinov, S. Amarie, W. Nuansing, F. Keilmann, R. Hilenbrand, *Nano Lett.* **2012**, *12*, 3973.
- [6] C. Wu, A. B. Khanikaev, R. Adato, N. Arju, A. A. Yanik, H. Altug, G. Shvets, *Nat. Mater.* **2012**, *11*, 69.
- [7] H. Hu, X. Yang, F. Zhai, D. Hu, R. Liu, K. Liu, Z. Sun, Q. Dai, *Nat. Commun.* **2016**, *7*, 12334.
- [8] K. Zhang, L. Zhang, F. L. Yap, P. Song, C. W. Qiu, K. P. Loh, *Small* **2016**, *1*, 1302.
- [9] D. C. Harris, *Materials for Infrared Windows and Domes: Properties and Performance*, SPIE Press, Cardiff, UK **1999**.
- [10] S. S. Chuang, M. A. Brundage, M. W. Balakos, G. Srinivas, *Appl. Spectrosc.* **1995**, *49*, 1151.
- [11] J. T. Yates, in *Experimental Innovations in Surface Science*, Springer, Berlin, Germany **2015**.
- [12] D. C. Harris, *Infrared Phys. Technol.* **1998**, *39*, 185.
- [13] D. C. Harris, in *Int. Symp. on Optical Science, Engineering, and Instrumentation, International Society for Optics and Photonics*, SPIE, Cardiff, UK **1995**.
- [14] J. M. Dawlaty, S. Shivaraman, J. Strait, P. George, M. Chandrashekar, F. Rana, M. G. Spencer, D. Veksler, Y. Chen, *Appl. Phys. Lett.* **2008**, *93*, 131905.
- [15] L. Falkovsky, *J. Phys.: Conf. Ser.* **2008**, *129*, 012004.
- [16] K. F. Mak, L. Ju, F. Wang, T. F. Heinz, *Solid State Commun.* **2012**, *152*, 1341.
- [17] K. F. Mak, M. Y. Sfeir, Y. Wu, C. H. Lui, J. A. Misewich, T. F. Heinz, *Phys. Rev. Lett.* **2008**, *101*, 196405.
- [18] T. Low, P. Avouris, *ACS Nano* **2014**, *8*, 16.
- [19] W. Xu, X. Ling, J. Xiao, M. S. Dresselhaus, J. Kong, H. Xu, Z. Liu, J. Zhang, *Proc. Natl. Acad. Sci. USA* **2012**, *109*, 9281.
- [20] I. Frank, D. M. Tanenbaum, A. van der Zande, P. L. McEuen, *J. Vac. Sci. Technol. B* **2007**, *25*, 2558.
- [21] K. Celebi, J. Buchheim, R. M. Wyss, A. Droudian, P. Gasser, I. Shorubalko, J.-I. Kye, C. Lee, H. G. Park, *Science* **2014**, *344*, 289.
- [22] J. S. Bunch, A. M. van der Zande, S. S. Verbridge, I. W. Frank, D. M. Tanenbaum, J. M. Parpia, H. G. Craighead, P. L. McEuen, *Science* **2007**, *315*, 490.
- [23] C. Chen, S. Lee, V. V. Deshpande, G.-H. Lee, M. Lekas, K. Shepard, J. Hone, *Nat. Nanotechnol.* **2013**, *8*, 923.
- [24] B. Zhang, Q. Li, T. Cui, *Biosens. Bioelectron.* **2012**, *31*, 105.
- [25] Y.-M. Chen, S.-M. He, C.-H. Huang, C.-C. Huang, W.-P. Shih, C.-L. Chu, J. Kong, J. Li, C.-Y. Su, *Nanoscale* **2016**, *8*, 3555.
- [26] H. Bethe, *Phys. Rev.* **1944**, *66*, 163.
- [27] C. Genet, T. Ebbesen, *Nature* **2007**, *445*, 39.
- [28] X. Huang, Z. Yin, S. Wu, X. Qi, Q. He, Q. Zhang, Q. Yan, F. Boey, H. Zhang, *Small* **2011**, *7*, 1876.
- [29] C.-K. Lee, Y. Hwangbo, S.-M. Kim, S.-K. Lee, S.-M. Lee, S.-S. Kim, K.-S. Kim, H.-J. Lee, B.-I. Choi, C.-K. Song, *ACS Nano* **2014**, *8*, 2336.
- [30] A. Das, S. Pisana, B. Chakraborty, S. Piscanec, S. Saha, U. Waghmare, K. Novoselov, H. Krishnamurthy, A. Geim, A. Ferrari, *Nat. Nanotechnol.* **2008**, *3*, 210.
- [31] Z. H. Ni, T. Yu, Z. Q. Luo, Y. Y. Wang, L. Liu, C. P. Wong, J. Miao, W. Huang, Z. X. Shen, *ACS Nano* **2009**, *3*, 569.
- [32] J.-B. Wu, H. Wang, X.-L. Li, H. Peng, P.-H. Tan, *Carbon* **2016**, *110*, 225.
- [33] J.-B. Wu, X. Zhang, M. Ijäs, W.-P. Han, X.-F. Qiao, X.-L. Li, D.-S. Jiang, A. C. Ferrari, P.-H. Tan, *Nat. Commun.* **2014**, *5*, 5309.
- [34] Z. Li, E. A. Henriksen, Z. Jiang, Z. Hao, M. C. Martin, P. Kim, H. Stormer, D. N. Basov, *Nat. Phys.* **2008**, *4*, 532.
- [35] J. Horig, C.-F. Chen, B. Geng, C. Girit, Y. Zhang, Z. Hao, H. A. Bechtel, M. Martin, A. Zettl, M. F. Crommie, *Phys. Rev. B* **2011**, *83*, 165113.
- [36] D. Rodrigo, A. Tittl, O. Limaj, F. J. G. de Abajo, V. Pruneri, H. Altug, *Light: Sci. Appl.* **2017**, *6*, e16277.
- [37] H. Yan, F. Xia, W. Zhu, M. Freitag, C. Dimitrakopoulos, A. A. Bol, G. Tulevski, P. Avouris, *ACS Nano* **2011**, *5*, 9854.
- [38] D. B. Farmer, D. Rodrigo, T. Low, P. Avouris, *Nano Lett.* **2015**, *15*, 2582.
- [39] T.-T. Tang, Y. Zhang, C.-H. Park, B. Geng, C. Girit, Z. Hao, M. C. Martin, A. Zettl, M. F. Crommie, S. G. Louie, *Nat. Nanotechnol.* **2010**, *5*, 32.
- [40] A. Kuzmenko, L. Benfatto, E. Cappelluti, I. Crassee, D. van der Marel, P. Blake, K. Novoselov, A. Geim, *Phys. Rev. Lett.* **2009**, *103*, 116804.
- [41] C. Lee, X. Wei, J. W. Kysar, J. Hone, *Science* **2008**, *321*, 385.
- [42] G.-H. Lee, R. C. Cooper, S. J. An, S. Lee, A. van der Zande, N. Petrone, A. G. Hammerberg, C. Lee, B. Crawford, W. Oliver, *Science* **2013**, *340*, 1073.
- [43] H. I. Rasool, C. Ophus, W. S. Klug, A. Zettl, J. K. Gimzewski, *Nat. Commun.* **2013**, *4*, 2811.
- [44] S. De, P. J. King, M. Lotya, A. O'Neill, E. M. Doherty, Y. Hernandez, G. S. Duesberg, J. N. Coleman, *Small* **2010**, *6*, 458.
- [45] T. Yoshihara, H. Tadokoro, S. Murahashi, *J. Chem. Phys.* **1964**, *41*, 2902.
- [46] A. Vakil, N. Engheta, *Science* **2011**, *332*, 1291.
- [47] V. P. Gusynin, S. G. Sharapov, J. P. Carbotte, *J. Phys.: Condens. Matter* **2007**, *19*, 026222.

Received: November 14, 2016

Revised: March 16, 2017

Published online: